

# How Phase Transitions Impact Changes in Mantle Convection Style Throughout Earth's History: From Stalled Plumes to Surface Dynamics

Ranpeng Li<sup>1</sup>, Juliane Dannberg<sup>1</sup>, Rene Gassmüller<sup>1</sup>, Carolina Lithgow-Bertelloni<sup>2</sup>, Lars Stixrude<sup>2</sup>

<sup>1</sup>Department of Geological Sciences, University of Florida, Gainesville

<sup>2</sup>Earth, Planetary, and Space Sciences, University of California, Los Angeles

## Key Points:

- For a mantle potential temperature above 1800 K, the wadsleyite to garnet (majorite) + ferropericlasite transition induces layering of plumes.
- The stalled plumes cause a long-lasting global temperature elevation at 500–650 km depth and reduce the vertical mass flux by up to 10%.
- As Earth transitions from the layering to a non-layering regime, the surface mobility increases.

---

Corresponding author: Ranpeng Li, [ranpeng.li@ufl.edu](mailto:ranpeng.li@ufl.edu)

## Abstract

Mineral phase transitions can either hinder or accelerate mantle flow. In the present day, the formation of the bridgmanite + ferropericlasite assemblage from ringwoodite at 660 km depth has been found to cause weak and intermittent layering of mantle convection. However, for the higher temperatures in Earth’s past, different phase transitions could have controlled mantle dynamics.

We investigate the potential changes in convection style during Earth’s secular cooling using a new numerical technique that reformulates the energy conservation equation in terms of specific entropy instead of temperature. This approach enables us to accurately include the latent heat effect of phase transitions for mantle temperatures different from the average geotherm, and therefore fully incorporate the thermodynamic effects of realistic phase transitions in global-scale mantle convection modeling. We set up 2-D models with the geodynamics software ASPECT, using thermodynamic properties computed by HeFESTo, while applying a viscosity profile constrained by the geoid and mineral physics data and a visco-plastic rheology to reproduce self-consistent plate tectonics and Earth-like subduction morphologies.

Our model results reveal the layering of plumes induced by the wadsleyite to garnet (majorite) + ferropericlasite endothermic transition (between 420–600 km depth and over the 2000–2500 K temperature range). They show that this phase transition causes a large-scale and long-lasting temperature elevation in a depth range of 500–650 km depth if the potential temperature is higher than 1800 K, indicating that mantle convection may have been partially layered in Earth’s early history.

## Plain Language Summary

Earth’s mantle convects, cooling the planet and driving the tectonic plates that shape the surface of the Earth. However, it is still an open question how the pattern of mantle convection has changed throughout Earth’s history. A key to answering this question might be the mineral assemblages in the mantle, which vary with depth due to changes in temperature and pressure. The transition between different mineral phases can affect the mantle flow and therefore the mantle convection style. For example, heat-absorbing transitions can result in denser mineral assemblages at higher temperatures, inhibiting mantle plumes—hot upwellings rising from the core-mantle boundary to the surface.

Our research investigates the influence of phase transitions on mantle plumes and convection style throughout Earth’s evolution through modeling. In the early stage of the Earth, when the mantle was hotter than today, different mineral phase transformations dominated the mantle. Our model shows that the transition from wadsleyite to garnet (majorite) + ferropericlasite can stop upwelling plumes, leading to elevated temperatures in a depth range of 500–650 km in a mantle that is hotter than in the present day. These results imply that mantle convection may have been partially layered early in Earth’s history.

## 1 Introduction

### 1.1 The Long-standing Puzzle of Mantle Convection Patterns

Understanding Earth’s mantle convection is crucial for reconstructing planetary evolution because the convection style is continuously shaping Earth’s mantle structure, chemical differentiation, mechanical mixing, cooling rate, and surface tectonic regimes. Although considerable insights into these processes have been gained over the past few decades from geochemical data, geophysical observations and dynamic models, many ques-

tions about how this convection style has evolved throughout Earth’s history remain unanswered.

Geochemical studies reveal different chemical reservoirs in the Earth’s interior. Plume-related oceanic island basalts sample a wide range of heterogeneity from the lower mantle (Zindler & Hart, 1986; White, 2015; Weis et al., 2023), including the primordial composition of the mantle (Graham, 2002; White, 2010; Jackson et al., 2010) and recycled crustal components (Hofmann & White, 1982; Weaver, 1991; Dasgupta et al., 2007), while the upper mantle has a more homogeneous composition that is depleted in incompatible elements and is the source of mid-ocean ridge basalt (Hofmann, 1988; Sun & McDonough, 1989). However, it is unclear where exactly in the lower mantle those heterogeneous reservoirs are located and how and to what extent they are preserved throughout Earth’s history.

Many studies have investigated mantle structure and mixing efficiency. The preservation of distinct reservoirs suggests the isolation of some primitive materials from a depleted and relatively well-mixed upper mantle. This has led to the idea that convection in the mantle could be layered (Richter et al., 1977; Hofmann, 1997). However, for the present-day style of convection, seismic observations show that slabs penetrate the transition zone and can reach the core-mantle boundary (Goes et al., 2017), where rising plumes originate (French & Romanowicz, 2015), suggesting whole-mantle convection. But the geophysical observations supporting whole-mantle convection for the present-day Earth do not exclude the potential occurrence of two-layered convection in the past. For example, Allègre (1997) calculates the geochemical mass flux and suggests that the average mass exchange between lower and upper mantle over the whole geological time is less than 10 % of the present-day slab flux. The lower mass flux in the past suggests that Earth might have convected in two layers during most of its history, and that whole-mantle convection might only have developed recently. However, this model is not favored since the mechanism for such dramatic change is unclear and no surface evidence is observed (van Keken et al., 2002). Moreover, several lines of geochemical evidence can not be explained by layered convection models (see review in van Keken et al. (2002)). The geochemical end-members in ocean island basalts are likely to reflect oceanic plates subducted in the past and the preservation of recycled surface components in the lower mantle (Hofmann & White, 1982). Coupled geodynamic/geochemical numerical models, such as Xie and Tackley (2004); Brandenburg et al. (2008), further support that the long-term recycling of ancient oceanic crust can reproduce EM-I and HIMU reservoirs that are similar to the ones found in geochemical analyses of ocean island basalts.

Consequently, many convection studies take into account both geophysical and geochemical observations and investigate the generation of chemical heterogeneity during whole mantle convection (van Keken et al., 2002). For example, Tackley (2000a) suggests that enriched components are embedded in the depleted mantle and melt at different temperature and pressure conditions. Bercovici and Karato (2003) proposed a transition-zone water filtering model, which can generate heterogeneous melt in a mantle convecting as a whole. Several studies also further investigate the preservation of chemical heterogeneity during the mantle’s mechanical mixing (Kellogg, 1992) and discuss mechanisms that can potentially promote layering of convection, such as phase transitions, viscosity jumps, and compositional variation. For example, endothermic phase transitions can hinder vertical mantle flow (for more details see Section 1.2). The effect of viscosity is more controversial: Some studies find that an increase in viscosity in the lower mantle leads to lower mixing efficiency (van Keken & Ballentine, 1999), while others do not see this effect (Naliboff & Kellogg, 2007). Inefficient mixing can be induced by rheological variations, either due to large lateral compositional difference of mantle materials (Kellogg et al., 1999) or higher viscosity blobs in kinematically driven flows (Manga, 1996; Becker et al., 1999). While some of the studies suggest a generally efficient mechanical mixing of the mantle in the past billions of years (van Keken & Zhong, 1999), some oth-

ers show the survival of heterogeneities (Ballmer et al., 2017; Gülcher et al., 2021). These models require further constraints, leaving many open questions about the convection patterns.

Moreover, the geological record suggests that the surface tectonic regime is evolving over time (Korenaga, 2013; Palin et al., 2020). Previous studies have proposed that Earth may have transitioned from a stagnant lid regime (Solomatov, 1995) to a mobile lid regime in the early Archean due to the potential weakening from melting (Loureño et al., 2020). But even after the onset of global plate tectonics, there were still changes in the convection style that are recorded by subduction-related metamorphism, the global zircon archive, and other surface records reflecting continent building (Brown & Johnson, 2018; Roberts & Spencer, 2015; Cawood & Hawkesworth, 2014; Palin et al., 2020). These variations in surface tectonics and the resulting crust production rate may relate to changes in deep mantle dynamics such as mantle avalanches, episodic subduction, or plumes (O’Neill et al., 2015), but the specific mechanism is not completely understood. In particular, it is still unclear how the mantle convection mode has evolved throughout Earth’s history, how it affects the onset of plate tectonics, and how it influences chemical differentiation and mixing of heterogeneities.

## 1.2 Phase Transitions Affect Convection Style

Mineral phase transitions have an important influence on mantle convection through their effect on buoyancy and latent heat. For example, endothermic transitions, which have a negative Clapeyron slope, can result in denser mineral assemblages at higher temperatures, inhibiting both upwelling plumes and downwelling slabs. Exothermic transitions have the opposite effect. The latent heat consumed or released during phase change can lead to abrupt changes in temperature across phase transitions and partially compensates the buoyancy effect. In addition to density, phase transitions also affect the viscosity of individual minerals and therefore the rock as a whole. For example, some phase transformations include dehydration reactions, which increase the material’s viscosity as water is released. Moreover, the average mantle viscosity is thought to change at the depth of major olivine phase transitions (Faccenda & Dal Zilio, 2017).

For the present-day mantle, major transitions include the transformation from olivine to wadsleyite at the 410 km discontinuity (positive Clapeyron slope), the transformation from wadsleyite to ringwoodite at the 520 km discontinuity (positive Clapeyron slope), and the transformation from ringwoodite to bridgmanite + ferropericlasite assemblage at 660 km depth (negative Clapeyron slope). There are many geodynamic modeling studies that have investigated the dynamic effect of these phase transitions. Christensen and Yuen (1985) systematically constrain the conditions for endothermic phase transitions to cause layered convection, suggesting that layering is facilitated more the larger the density jump, the more negative the Clapeyron slope, and the higher the Rayleigh number. With a negative Clapeyron slope of approximately  $-0.5$  to  $-4$  MPa/K, the phase transition at 660 km has been suggested to cause slab stagnation, the accumulation of cold downwelling material followed by avalanches, and weak intermittent layering of mantle convection (Christensen & Yuen, 1984; Machetel & Weber, 1991; Peltier & Solheim, 1992; Tackley et al., 1993; Goes et al., 2017). Brunet and Yuen (2000); Marquart et al. (2000); Bossmann and van Keken (2013) show that plumes may partially stall in the transition zone due to the negative buoyancy and phase-dependent viscosity. Moreover, Tosi and Yuen (2011) suggest that the viscosity contrast between lower and upper mantle can cause plumes to spread laterally as channel flows. Liu et al. (2018) further include the effect of the post-garnet transition, and suggest that the combined phase transitions can trap low-temperature plume material and form plumes with complex morphologies.

For the higher temperatures in Earth’s past, however, different phase transitions might have controlled mantle dynamics, implying a change in convection patterns dur-

ing Earth’s secular cooling. Figure 1 shows a mineral phase diagram of a pyrolitic bulk composition computed by the thermodynamics software HeFESTo (Wei et al., 2020; Stixrude & Lithgow-Bertelloni, 2011). This phase diagram includes the transformation from wadsleyite to garnet (majorite) + ferropericlasite between 420–600 km depth and over the 2000–2500 K temperature range, which is only encountered by material moving along a hot mantle adiabat in the transition zone. This phase transformation has only been investigated by very few studies. Ichikawa et al. (2014) suggest that this phase transition can affect hot plumes especially for models with a high CMB temperature. Stixrude and Lithgow-Bertelloni (2022) highlight the strongly negative phase buoyancy parameter of this transition and discuss its potential influence on hindering plumes in the early Earth. However, open questions remain about the timing and degree of such impedance effects. Under what conditions can the wadsleyite to garnet (majorite) + ferropericlasite affect mantle flow? Is the potential impedance strong enough to cause layered convection? How would it affect plume morphologies and mantle convection style when taking into account the potential effect of other major phase transitions? Therefore, models that can represent different stages of Earth’s secular cooling and incorporate the corresponding change in phase assemblage in a realistic way are needed to further investigate these questions.

In this paper, we present a numerical modeling study that reveals the influence of phase transitions on mantle convection throughout Earth’s cooling history. In Section 2, we discuss our new entropy method, model setup, and parameter choices. In Section 3, we present the results from our global mantle convection models. We characterize their plate-like behavior and compare them with observations to show that they are a reasonable approximation of Earth. We also quantify the layering effect of the wadsleyite to garnet (majorite) + ferropericlasite phase transition, which occurs in models with high mantle temperature. In Section 4, we discuss the effect of different phase transitions on mantle convection during Earth’s secular cooling, and its potential link to surface tectonics and the chemical differentiation of mantle plumes.

## 2 Methods

### 2.1 Governing Equations

To capture sharp and broad transitions in a multi-phase assemblage and accurately model the full dynamic and latent heat effects of phase transitions, we follow the entropy method for geodynamic modeling of phase transitions described in detail in Dannberg et al. (2022).

With this method, we solve the momentum conservation equation,

$$-\nabla \cdot (2\eta\dot{\epsilon}) + \nabla p = \rho\mathbf{g}, \quad (1)$$

mass conservation equation,

$$\frac{\partial \rho}{\partial t} + \mathbf{u} \cdot \nabla \rho + \rho \nabla \cdot \mathbf{u} = 0, \quad (2)$$

and the energy equation in pressure–entropy space,

$$\rho T \left( \frac{\partial S}{\partial t} + \mathbf{u} \cdot \nabla S \right) + \rho C_p \frac{\partial T}{\partial t} \Big|_{cond} = \rho Q + 2\eta\dot{\epsilon} : \dot{\epsilon} \quad (3)$$

All symbols are explained in Table 1.

To include the effects of compressibility while avoiding pressure oscillations, we apply the Projected Density Approximation (Gassmöller et al., 2020), which uses the hydrostatic reference pressure to compute density, but otherwise takes into account all dynamics effects in the mass conservation equation instead of using a reference density profile. We use a matrix-free geometric multi-grid method for solving the Stokes system (Clevenger

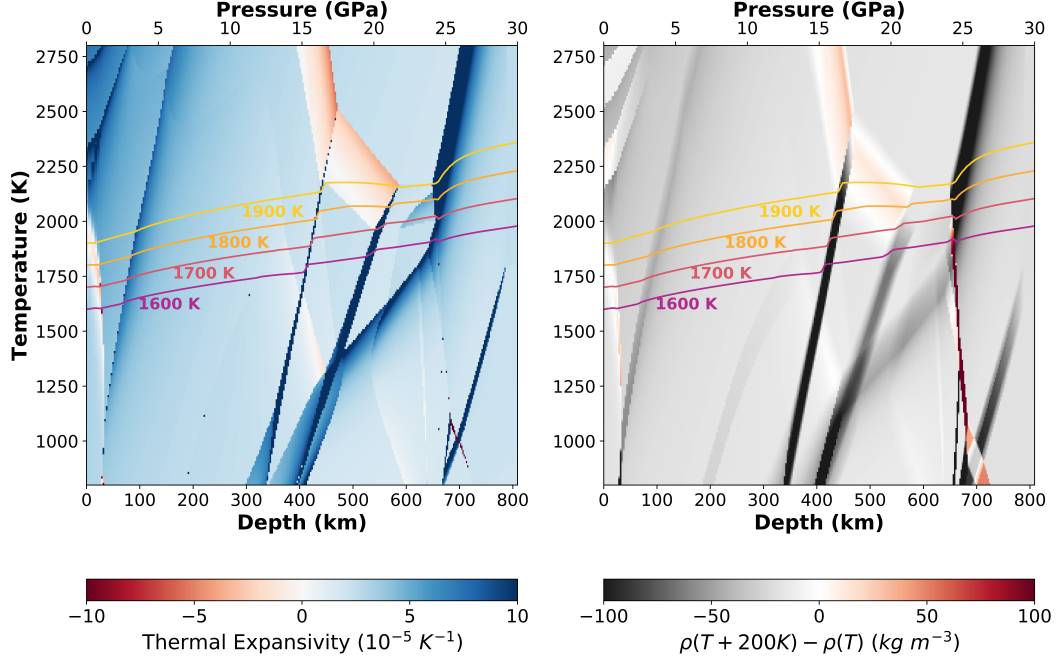


**Figure 1.** Material properties of the pyrolite composition used in this study. Left: thermal expansivity in dependence of pressure (x-axis) and temperature (y-axis). The spikes indicate phase transitions. Right: Density variations between two points in the material table with the same pressure, but a temperature difference of 200 K. For a plume with an excess temperature of 200 K, colors illustrate its density difference compared to the background mantle. At the phase transitions that stand out in red color, the plume is denser than the ambient mantle and therefore impeded. Isentropes for different mantle potential temperatures are plotted as solid lines in yellow to purple color.

**Table 1.** Symbols in the equations and their meaning

Symbol	Meaning	Value
$S$	entropy	solution variable
$\mathbf{u}$	velocity	solution variable
$T$	temperature	computed with HeFESTo
$\rho$	density	computed with HeFESTo
$\alpha$	thermal expansion coefficient	computed with HeFESTo
$\eta$	viscosity	computed with reference profile <sup>a</sup>
$p$	pressure	solution variable
$C_p$	specific heat capacity	computed with HeFESTo
$\mathbf{g}$	gravity	$9.8 \text{ m s}^{-2}$
$Q$	intrinsic heat production	$2.09 \times 10^{-12} \text{ W kg}^{-1}$ <sup>b</sup>
$\dot{\epsilon}$	strain rate	solution variable
$k$	Thermal conductivity	$4.7 \text{ W m}^{-1} \text{K}^{-1}$ <sup>c</sup>

<sup>a</sup> Reference viscosity profile from Steinberger and Calderwood (2006)

<sup>b</sup> Heating rate for depleted mantle (Korenaga, 2017)

<sup>c</sup>  $k$  is used to compute thermal diffusion, see Dannberg et al. (2022) Eq.12

& Heister, 2021). As the material properties depend on entropy, pressure and strain rate, our equations are strongly non-linear, and we therefore apply an iterative solution method using a nonlinear solver. A detailed description of the numerical problem along with several benchmark cases can be found in Dannberg et al. (2022), and the current study is the first application of this method to large-scale Earth-like convection simulations. Our model setup builds on the example spherical convection models shown as a proof-of-concept in Dannberg et al. (2022), Section 3.3. The main improvement is the formulation of the rheology (see details in Section 2.4), which now allows for plate tectonics in the models (see discussion in Section 3.1).

## 2.2 Model Setup

We set up 2D cylindrical annulus models with an inner radius of 3481 km and an outer radius of 6371 km. The models have uniform mesh cells, with 128 cells in radial and 1536 cells in lateral direction. This results in a mesh cell size of  $14.2 \text{ km} \times 22.6 \text{ km}$  at the core-mantle boundary (CMB) and  $26.1 \text{ km} \times 22.6 \text{ km}$  at the surface. Both boundaries are free-slip. This results in a rotational nullspace, which we remove by setting the net rotation to zero. The boundary temperatures are prescribed through entropy: At the surface, we set the entropy to be  $656 \text{ J/kg/K}$ , corresponding to a temperature of 300 K at 0 GPa. The prescribed entropy of the CMB varies for different models, and the corresponding values are shown in Table 2. The models are in a mixed heating mode, which includes both the basal heating from the inner boundary, and a contribution of isotopic radiogenic heating of  $2.09 \times 10^{-12} \text{ W kg}^{-1}$  (suggested for depleted mantle by Korenaga (2017)) throughout the model domain.

The model temperature is initialized as an adiabat, with the potential temperatures for the different models given in Table 2 and the following anomalies: The temperature in the thermal boundary layers at the top and bottom of the adiabatic mantle is based on a half-space cooling model assuming a cooling time of 50 Myr. In addition, we set a sinusoidal entropy perturbation with an amplitude of  $\pm 10 \text{ J/kg/K}$ , a lateral wave number of 2, and a radial wave number of 0.5 (i.e., two hot and two cold anomalies in a circular wave pattern) to make the wavelength of the initial up- and downwellings independent of numerical noise. We also apply a single Gaussian perturbation at the CMB with a sigma of  $\pi/50$  and an amplitude equaling the entropy jump across the bottom thermal boundary layer. This leads to a similar size and temperature distribution as within the first plume head that would initiate at the CMB in a model with the same setup but no perturbation and makes the first plume rise earlier so that the models enter a steady state faster.

We here show two different types of models: (1) A series of 8 quasi-steady state models (500 Myr model evolution time) with a broad range of core-mantle boundary temperatures and starting mantle adiabats, which represent Earth at different stages of cooling, and (2) A long-term model (3 Gyr model evolution time) with Earth-like thermal evolution, showing the changes in convection style during the transition from a hotter to a colder mantle. All models presented in this study are simulated with the community geodynamic modeling code ASPECT version 2.5.0 (Heister et al., 2017; Kronbichler et al., 2012; Bangerth et al., 2023b, 2023a).

## 2.3 Equation of State

Our models assume a homogeneous pyrolitic composition, an equilibrium assemblage of 18% basalt and 82% harzburgite (Xu et al., 2008). We use a lookup table in which material properties such as density, temperature, and specific heat change in pressure-entropy space. The material properties are computed with the global Gibbs free energy minimization code HeFESTo (Stixrude & Lithgow-Bertelloni, 2005, 2011), using a dataset

**Table 2.** Model parameters

Model name	Entropy of starting adiabat ( $\text{J kg}^{-1}\text{K}^{-1}$ )	Corresponding potential temperature (K)	Prescribed entropy at CMB ( $\text{J kg}^{-1}\text{K}^{-1}$ )	Corresponding CMB temperature (K)
1600-3800	2535.08	1600	2956.187	3800
1600-4000	2535.08	1600	3021.448	4000
1700-3900	2613	1700	2999.183	3900
1700-4100	2613	1700	3052.99	4100
1750-4200	2650.672	1750	3084	4200
1770-3800	2665.556	1770	2956.187	3800
1800-4000	2687.748	1800	3021.448	4000
1800-4200	2687.748	1800	3084	4200
1900-4100	2760.4	1900	3052.99	4100
1900-4300	2760.4	1900	3114.06	4300
1900-cools	2760.4	1900	3099.03	4250 <sup>a</sup>

<sup>a</sup> Starting with 4250 K, the CMB temperature decreases by 500 K over 3 Gyr

from Wei et al. (2020). This dataset used the composition from Xu et al. (2008) and updated parameters from Stixrude and Lithgow-Bertelloni (2011).

In Figure 1, we visualize this material table, illustrating changes in thermal expansivity and density differences between adiabats, and highlighting the phase transitions. In this material table, the olivine to wadsleyite transition that occurs around 410 km depth has a Clapyeron slope of  $\sim 3.4$  MPa/K. The phase transition from ringwoodite to bridgmanite + ferropericlasite at around 660 km depth has a Clapyeron slope of  $\sim -1.4$  MPa/K.

## 2.4 Rheology

The viscosity in our models is both depth- and temperature-dependent (Figure 2). We interpolate the preferred viscosity profile of Steinberger and Calderwood (2006) (using a linear interpolation of the logarithm of the viscosity profile M1b in figure 13) to compute a smooth profile for the radial variations. While the viscosity for the starting adiabat  $T_{adi}$  follows this radial profile ( $\eta_{adi}$ ), the viscosity for temperatures away from the starting adiabat is re-calculated according to Equations (5) and (6) in Steinberger and Calderwood (2006):

$$\eta(T) = \eta_{adi} \exp \left( -\frac{H(T - T_{adi})}{nR(TT_{adi})} \right) \quad (4)$$

where  $H$  is the activation enthalpy and  $R = 8.314 \text{ J/(mol K)}$  is the gas constant.  $H/(nR)$  also varies with depth as given in Steinberger and Calderwood (2006). The stress exponent is  $n = 3.5$  above 660 km depth (assuming dislocation creep), and  $n = 1$  below 660 km depth (assuming diffusion creep).

This profile is constrained by mineral physics data and geoid data of the present-day Earth. For our models starting with a higher background adiabat representing Earth in the past, we recalculate the viscosity profile according to the temperature differences between different adiabats (solid lines in Figure 2). For computational efficiency, we limit the maximum lateral viscosity variations of our quasi-steady state models to a factor of 2000 from the reference profile (dashed lines in Figure 2). For the long-term model, which has temperatures evolving further away from the initial adiabat, we limit lateral vari-

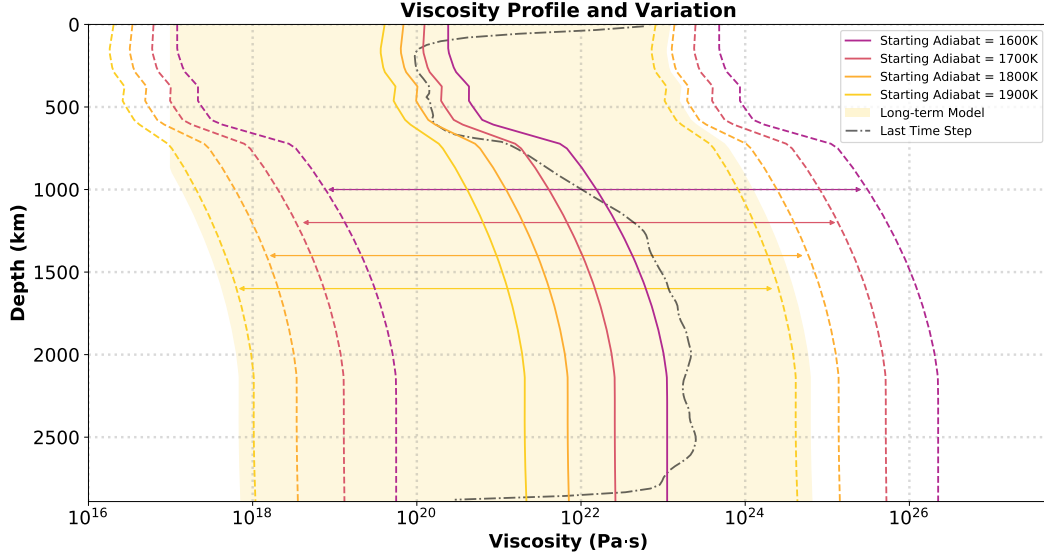


**Figure 2.** Viscosity profiles. Solid lines: Reference viscosity profile of models with different starting adiabats. Dashed lines: lower and upper limit of the viscosity of the quasi-steady state models. Shaded area: viscosity variation of the long-term model. Dash-dotted line: The laterally averaged viscosity of the long-term model at the end of its evolution (3 Gyr).

ations to a factor of 3000, while also applying a lower limit of  $10^{17}$  Pa s and an upper limit of  $10^{25}$  Pa s (shaded area in Figure 2).

To reproduce self-consistent plate tectonics with subduction in our geodynamic model, we also include plastic yielding in our rheology. When the stress applied to the rock reaches the yield strength at depth, the rock fails. We approximate this by reducing the viscosity until the stress is exactly at the yield strength;  $\tau = \tau_{yield}$ . Below the yield strength, the material deforms viscously ( $\tau = 2\eta\dot{\epsilon}$ ). The yield strength is determined according to the Drucker–Prager criterion:

$$\tau_{yield} = p_h \sin(\phi) + C \cos(\phi) \quad (5)$$

where  $p_h$  is the hydrostatic reference pressure,  $C$  is the cohesion (Pa) and  $\phi$  is the angle of internal friction. The larger the cohesion, the higher stresses are required to break the plate at the surface. The higher the friction angle, the more difficult it becomes to break the plate at increasing depth. We choose a cohesion of 80 MPa and a friction angle of 0.005 (in radians). This combination of parameters achieves a surface velocity and plate morphology close to the Earth. We discuss this in more detail in the Results section, where we compare model statistics with observations.

## 3 Results

### 3.1 Plate-like Behavior

We present results from 8 quasi-steady state models with different starting adiabatic temperatures and CMB temperatures that represent different stages of Earth’s cooling, and one long-term model illustrating 3 Gyr of secular cooling. Their entropy and corresponding temperature setup is described in detail in Table 2.

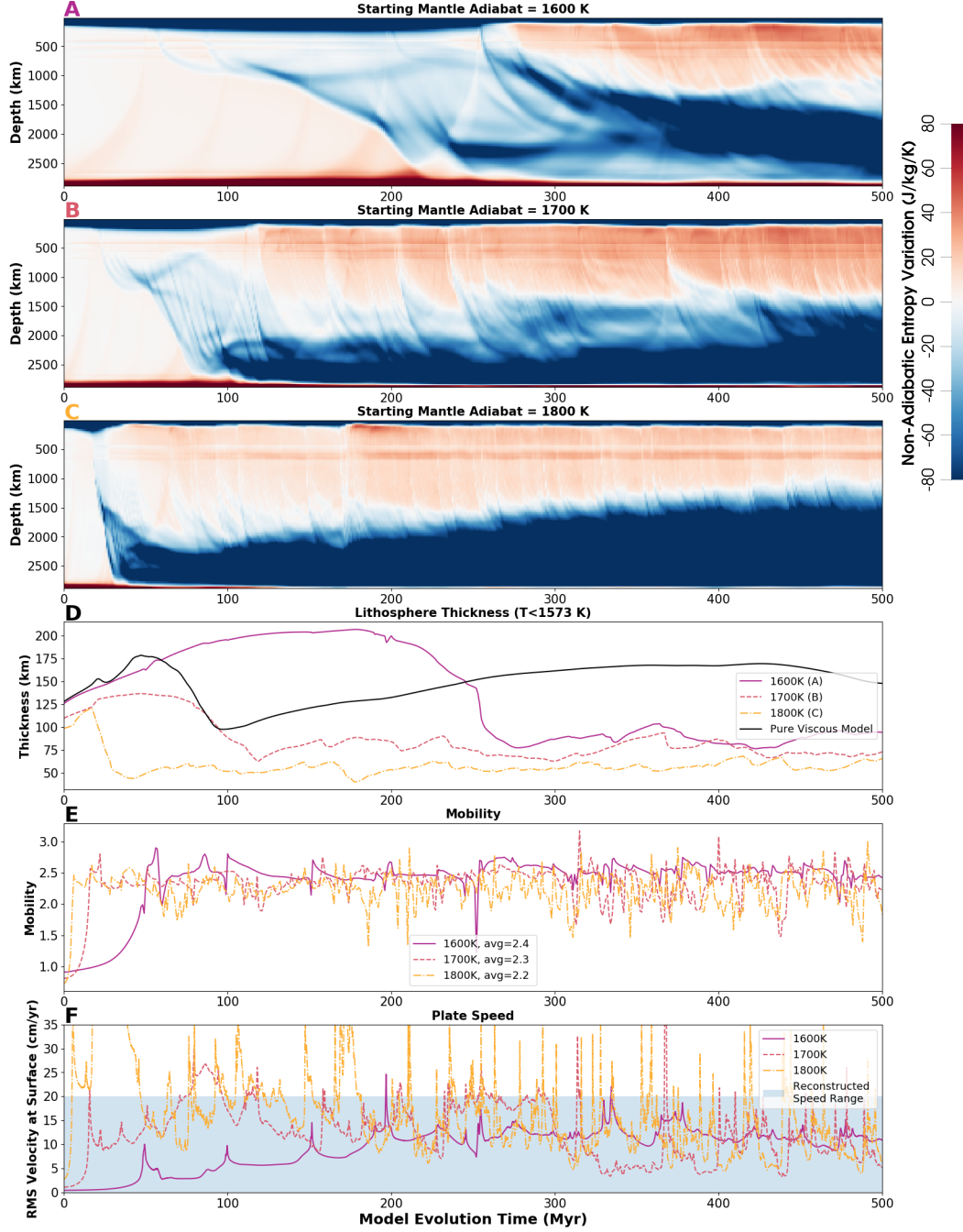


**Figure 3.** A-C: Deviation of the laterally averaged entropy from the initial starting adiabat of convection models 1600-4000 (panel A), 1700-4100 (panel B), and 1800-4200 (panel C), plotted over the model evolution time. Red and white streaks that slope upwards mark rising plumes. Blue streaks sloping downwards record subducting slabs. The high entropy area just below the top boundary illustrates accumulated hot plume material. The low entropy in the lower mantle is built up by cold subducted slabs. D: Averaged lithosphere thickness plotted over the model evolution time for the models shown in A-C (colored lines) and a purely viscous model that has a starting adiabat of 1600 K. The lithosphere thickness is determined by the 1573 K isotherm. E: Model mobility plotted over the evolution time for the three models shown in A-C. Mobility is defined as surface RMS velocity divided by the RMS velocity of the whole model. F: Averaged plate speed plotted over the model evolution time for the three models shown in A-C. The shaded area shows the range of reconstructed plate speeds inferred from paleomagnetic data in Zahirovic et al. (2015).

### 3.1.1 *Quasi-Steady State Models with Present-Day Earth Conditions*

We first compare the lithospheric thickness, mobility, and surface velocity of the model setup corresponding to the present-day (1600-4000, Figure 3D, solid purple line) to observations to show that our models are a reasonable approximation of mantle convection and plate tectonics on Earth. To calculate the lithosphere thickness in our models, we define a purely thermal lithosphere that is bounded by an isotherm of 1573 K (Artemieva, 2006). For today's Earth, the thermal oceanic lithosphere thickness averages around 80 km (Rychert et al., 2020). Seismic observations also suggest that the oceanic lithosphere has a monotonic subhorizontal profile at 70–80 km, and it rarely exceeds 135 km (Burgos et al., 2014). In our model 1600-4000, which has a starting adiabat of 1600 K, the lithospheric thickness stays within the observed range after the model enters the quasi-steady state at approximately 250 Myr.

To characterize the plate-like behavior of our models, we use mobility as a quantitative diagnostic (Tackley, 2000b). Mobility is defined as the ratio of the surface root-mean-square (RMS) velocity and the whole model RMS velocity. In an isoviscous model without rigid plates, the surface and the mantle move at a similar speed, thus resulting in a mobility of around 1. In a purely viscous model with temperature-dependent viscosity (for example, the spherical model presented in Dannberg et al. (2022)), a stagnant lid forms at the surface, thus resulting in a mobility of less than 1. For models with plate tectonics, the rigid plates at the surface subduct and move faster than the underlying mantle. Thus, a mobility larger than 1 suggests the occurrence of plate tectonics. In all our models, the mobility is  $\gg 1$  at all times (Figure 3E). This suggests that our chosen rheology generates plate tectonics in the models.

We also compare Earth's plate velocity to our model results (Figure 3F, solid purple line). The model plate velocity is computed by averaging the velocity along the outer boundary. Zhirovic et al. (2015) suggest that plates with a lower fraction of continental area move faster and that purely oceanic plates can reach speeds of 20 cm/yr. Our model velocities range from 0-25 cm/yr, and they generally fall into the range of 0-20 cm/yr except for two short-lived peaks that are caused by new subduction initiations. As our models do not include continents, the models' surface velocity is more comparable to oceanic plates rather than the global average.

The match between our models and observations for all three criteria suggests that these models are a reasonable representation of the Earth's deformation behavior. As a next step, we will analyze the statistical variations between different models to reveal how mantle convection evolved with the cooling of the Earth.

### 3.1.2 *Quasi-Steady State Models Representative of Earth's Past*

As Earth's mantle is cooling over time (Herzberg et al., 2010), models that have mantle adiabats with a higher potential temperature better represent Earth in the past. Comparing the different quasi-steady state models shows that the models with a higher starting adiabat have a thinner thermal lithosphere (Figure 3D) and higher plate velocities (Figure 3F). This is because the higher temperature causes a lower viscosity and therefore a larger Rayleigh number and more vigorous convection across various scales. At shallow depth, this effect leads to increased small-scale convection beneath the cold plates, thinning the lithosphere by removing material from its base. On the whole-mantle scale, the more vigorous convection results in more frequent subduction—causing more spikes in the speed of plate motion as shown in Figure 3F—and therefore on average younger (and thinner) plates. This change in convection style also affects the mobility, as discussed in Section 4.

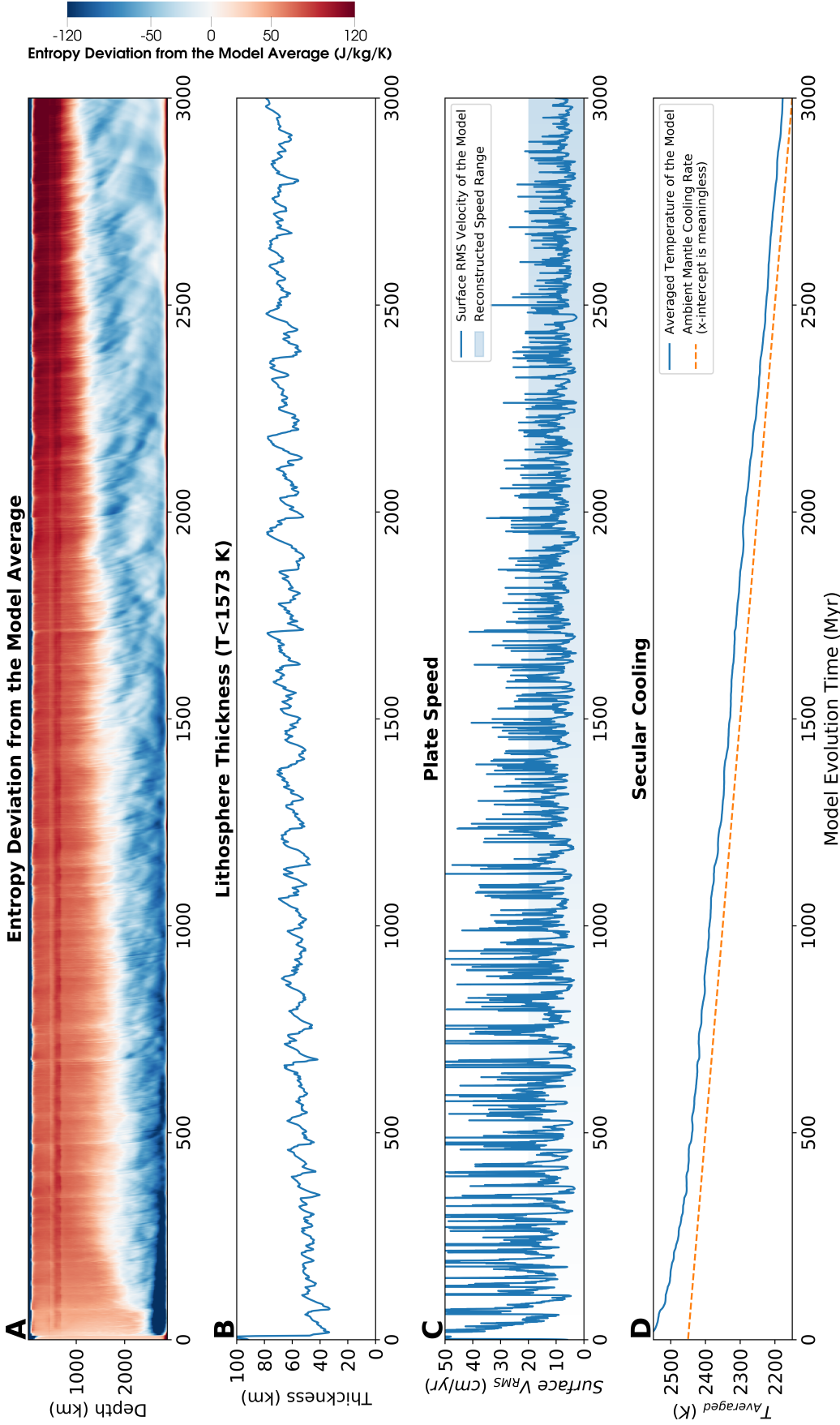


**Figure 4.** Results of the long-term model 1900-cools. A: Deviation of the laterally averaged entropy from the average entropy of the whole model domain, plotted over the model evolution time. Since the average model entropy decreases over the model evolution time of 3 Gyr, the thermal features are better illustrated by plotting the deviation from the model average instead of from the initial adiabat. B: Averaged lithosphere thickness (depth of the 1573 K isotherm) plotted over the model evolution time. C: Average plate speed plotted over the model evolution time. The shaded area shows the range of reconstructed plate speeds from (Zahirovic et al., 2015), with uncertainties increasing for earlier stages of Earth's history. D: Averaged model temperature plotted over the evolution time (blue line). The temperature decreases by about 100 K per Gyr (orange line), which is consistent with Earth's cooling history suggested by the petrological record (Herzberg et al., 2010). The video of the full evolution of this model can be found in supplementary video 1 (<https://youtu.be/-85MbYwC2fI>).

342

### 3.1.3 Cooling Model with a Decreasing CMB Temperature

343

344

345

346

347

348

349

We also present a long-term model that shows the change of convective behavior described in the previous section more gradually (Figure 4). This model cools from a potential temperature of 1900 K to around 1600 K in 3 Gyr. This cooling rate is consistent with the secular cooling of Earth suggested by petrology studies (Herzberg et al., 2010; Condie et al., 2016). This long-term model shows the same trends as the individual quasi-steady state models: The lithospheric thickness increases over time; the mobility increases over time; and the plate speed decreases over time.

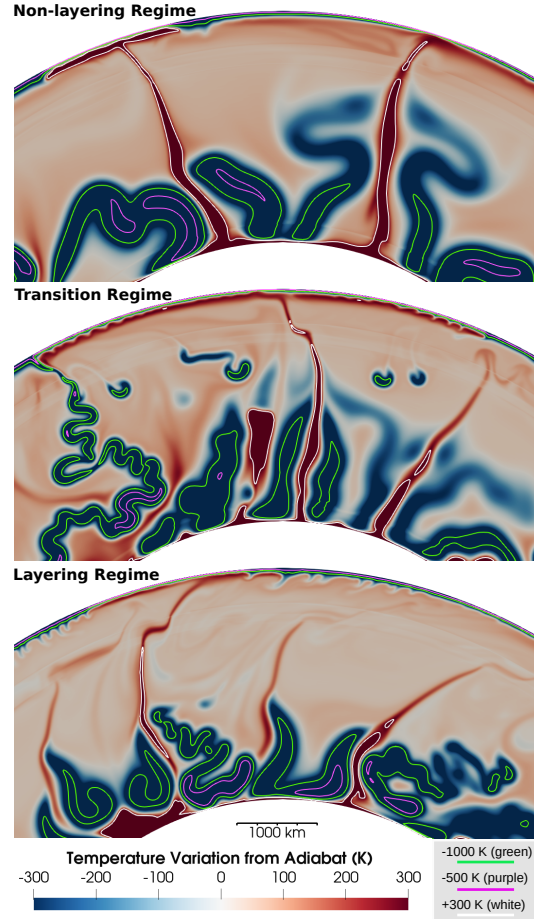


**Figure 5.** Snapshots of three models that fall into three different convection regimes. The colors show the temperature deviation from the starting adiabat. To clearly show the plumes, the color scale is limited to  $\pm 300$  K, concealing the lower temperatures in subducted slabs and making them appear thicker than they are. Isotherms of -1000 K, -500 K, and 300 K are highlighted as green, purple, and white lines. Top: Model 1600-4000 (Panel A in Figure 3) at 400 Myr. Middle: Model 1700-4100 (Panel B in Figure 3) at 330 Myr. Bottom: Model 1800-4200 (Panel C in Figure 3) at 210 Myr.

350

## 3.2 Layering, Transition, and Non-Layering Regimes

351

352

Above we have shown that the quantitative measures describing convection and plate motions change between models with different mantle temperatures. In the following,

we will demonstrate that these models also feature different convection styles, mantle thermal structure, and plume morphologies.

The most prominent feature expressing these variations in convection style is the layering of plumes in the transition zone, which is caused by the impedance of the phase transition wadsleyite = garnet (majorite) + ferropericlase (see Figure 1, Section 1.2). Accordingly, plumes in our models can be classified into three regimes: layering, transition, and non-layering. In Figure 5, we show three snapshots from three models: 1600-4000, non-layering regime (top); 1700-4100, transition regime (middle); and 1800-4200, layering regime (bottom). Plumes in the non-layering regime rise straight to the base of the lithosphere. In the transition regime, most plumes rise directly, while a few of them are slightly deflected by the phase transition at around 500 km depth. The larger the tilt of a plume, the more likely it is that it will be impeded and begin to show layering. However, this layering does not last for a long time and has limited influence on the long-term thermal structure. In the layering regime, more than half of the plumes are being stalled in the transition zone. Although most of the plume heads still reach the surface, their conduits are tilted very strongly in a short amount of time. This often cuts off the plume and traps the layered conduit right below 500 km depth for a long period of time. As a separated high-temperature layer forms at that depth, we also observe more secondary plumes rising from this layer.

The layering of plumes also affects the models' large-scale thermal structure. Figure 3A-C shows the depth-averaged entropy plotted over the model evolution time for the same three quasi-steady state models (with different initial adiabats) as shown in Figure 5. The blue streaks sloping downwards are cold sinking slabs, which eventually accumulate in slab graveyards at the base of the mantle (dark blue layer in the bottom half of each panel). The red streaks sloping upwards are hot rising plumes. As shown in Figure 3, panels A-C, all three models feature a layer of elevated entropy (corresponding to higher temperatures) at the base of the lithosphere, where plumes spread laterally and accumulate in the asthenosphere. However, only the model with an initial adiabat of 1800 K (panel C) has another layer of elevated entropy at 500-650 km depth (indicated by darker shades of red). This layer is generated by plumes that are impeded by the phase transition wadsleyite = garnet (majorite) + ferropericlase, as shown in Figure 5. The same layer with elevated entropy is also present in the first 2 Gyr of the long-term cooling model, when the potential mantle temperature is above 1700 K (see Figure 4).

To quantitatively show the existence of layering, we compute how the laterally averaged vertical mass flux and velocity reduction change along a vertical profile through the mantle. Based on the shape of this profile, we define the range of the layering (blue), transition (orange), and non-layering (grey) dynamic regimes (Figure 6). In the convection models with no layering, the vertical mass flux continuously increases from the CMB to the asthenosphere (Figure A1 in Appendix). In the layering regime, the reduction of mass flux is strong enough to create a local minimum around 550-600 km depth. The quasi-steady state models with a starting adiabat of 1600 K do not show an obvious mass flux or velocity reduction, and they fall into the non-layering regime. The models with starting adiabats of 1800 and 1900 K all feature a strong mass flux reduction, and they fall into the layering regime. The models with a starting adiabat of 1700 K do not have a strong mass flux reduction that could yield a local minimum. However, these models show a visible reduction in the vertical velocity (orange lines in Figure 6A), suggesting that some weak layering occurs. We therefore classify these models as being in a transitional regime. For our long-term model that runs for 3 Gyr, we average every 300 Myr of the model evolution time (Figure 6B). Applying the same criteria, the first 1500 Myr of the model fall into the layering regime, the next  $\sim 900$  Ma are in transition regime, and the later stages of the model are in the non-layering regime.

Figure 6C shows a regime diagram that illustrates the mantle potential temperature range associated with each regime together with the degree of layering in each model.

Represented by both the size and color of the circles, we define the degree of layering in the following way: The reduction of mass flux causes a local minimum and two neighboring local maxima. We obtain the unreduced mass flux by linearly interpolating between the local maxima. We then use the difference between the local minimum and the interpolated value at the same depth as the reduction caused by the phase transition, and calculate its percentage with respect to the unreduced mass flux. In the layering regime (blue background color), both higher adiabatic temperatures and higher CMB temperatures cause more layering. For our long-term model that cools around 100 K per Gyr, we again average every 300 Myr of the model evolution time, and plot them according to their potential mantle temperatures in the regime diagram. This series of colored circles shows the same trend as the quasi-steady state models: the layering decreases over the model evolution time as the mantle cools down. Both model series leave the layering regime and enter the transition regime (orange background color) as their mantle potential temperature falls below around 1750 K. They then enter the non-layering regime (grey background color) when the mantle potential temperature is between 1700 and 1650 K.

The changes between regimes are also obvious in Figure 6, panel D. In this figure, we plot the spatial derivative of the laterally averaged vertical velocity and how this 1D profile evolves over time in the long-term model. When there is no layering in the convecting mantle, the material ‘accelerates’ as it rises, so the vertical velocity variation is larger than zero (color change from lighter to darker shades of red with decreasing depth) until it reaches the bottom of the lithosphere (Figure 6, panel D, grey box). When the phase transition impedes plumes even only to a small degree, the ‘acceleration’ is negative (orange box in Figure 6D). In this case, the vertical velocity variation is smaller than zero (light blue colors around 650–700 km depth). The larger and darker blue areas in the transition zone at earlier model evolution times (blue box in Figure 6D) suggest a stronger layering effect. This figure presents the gradual change between different regimes. We observe that the velocity reduction below 500 km depth becomes smaller over time, and eventually disappears after 2200 Myr as the model enters a non-layering regime.

### 3.3 Effect of Viscosity

Because our models include the effect of changes in mantle potential temperature on both phase transitions and mantle viscosity, the quasi-steady state models each have different reference viscosities. In the models with starting adiabats higher than 1600 K, the viscosity profile has been recalculated according to the temperature differences between adiabats (see Figure 2). Therefore, the models with a higher starting adiabat have a lower viscosity. This results in thinner plume conduits and slabs and more vigorous convection in the models with a hotter adiabat (Figure 3, and as discussed in Section 3.1.2). The reduced viscosity also causes these models to enter the quasi-steady state faster, since the first plume rises earlier and the average velocity is larger.

For the long-term model, the average mantle viscosity changes over time. The model has a low initial viscosity profile as it starts with an adiabat of 1900 K. As the model cools over time, the decreasing temperature increases the viscosity throughout the model domain. After 3 Ga, as the model cools to around 1600 K, the viscosity output (dash-dotted black line in Figure 2) shows a similar trend as the observed viscosity for today’s Earth (Steinberger & Calderwood, 2006).

Even though the viscosity may affect the degree of mass flux reduction, layering of plumes for high potential temperatures occurs regardless of the viscosity formulation. This was a result of our earlier study (Dannberg et al., 2022), where models with a constant reference viscosity and a hotter mantle potential temperature also featured the stalling of plume material due to the wadsleyite to garnet (majorite) + ferropericlasite phase transition. In the current study, we further demonstrate the existence of layering for higher

mantle temperatures taking into account the combined effect of the changes in phase transitions and an Earth-like rheology.

## 4 Discussion

We have shown that the convection style is expected to change as the Earth's mantle is cooling, because of both a changing viscosity and the prevalence of different mineral phase transitions at different mantle potential temperatures. In the following, we will discuss the impact of different phase transitions on mantle dynamics in different time periods of Earth's history. Sections 4.1 to 4.4 will focus on the influence of the wadsleyite to garnet (majorite) + ferropericlasite transition on Earth's thermal and chemical evolution. In Section 4.5, we will discuss the effect of other major phase transitions in the mantle.

### 4.1 Partial Impedance of Mass Exchange

Our convection simulations show that the occurrence of the wadsleyite to garnet (majorite) + ferropericlasite phase transformation at higher mantle potential temperatures in the Earth's past likely led to the deflection and layering of plumes at 500 km to 600 km depth. This layering also reduces the mass exchange between the upper and the lower mantle. However, the impeding effect of the transition is not very strong and the reduction only reaches up to 10% of the total vertical mass flux. Therefore, this effect is not strong enough to result in completely layered convection with separate convection cells above and below the transition. Moreover, the absolute value of the vertical mass flux becomes smaller as the mantle cools and the average velocity decreases over time (see Figure 6A). Therefore, the amount of mass exchange between the upper and the lower mantle is higher in the hotter layering regime compared to the non-layering regime in the colder mantle, even with the partial mass flux reduction.

### 4.2 Elevated Temperature in the Transition Zone

In the layering regime, the stagnant plumes caused by the wadsleyite to garnet (majorite) + ferropericlasite phase transformation cause an entropy increase between 500 km and 600 km depth. Locally, the stalled plume heads can raise the temperature to around 40-250 K above the adiabat. Another contribution to the entropy increase comes from the heat diffusion at endothermic phase transitions, where along the adiabat there is a temperature drop, and therefore diffusion causes a small positive entropy anomaly and a temperature increase just below the transition compared to the initial adiabatic temperature. With both impeded plumes and the conduction along the adiabat, the globally averaged total entropy changes up to  $\sim 10$  J/kg/s, which is equivalent to a temperature elevation of around 9.5 K above the adiabat. This entropy and temperature elevation can change the thermal profile in the transition zone to a minor degree.

### 4.3 Variation in Surface Mobility

All of our models produce plate-tectonic style convection with subducting slabs, regardless of the model evolution time. However, our models show a general trend that the surface mobility increases as the mantle potential temperature becomes lower and enters the non-layering regime. In the quasi-steady state series, models with lower potential temperature have a higher averaged surface mobility (Figure 3 E, the average mobility is noted in the legend). Moreover, the long-term model shows a significant increase of surface mobility as the model enters a non-layering state (Figure 7), illustrated by the abrupt change in the slope of the mobility trend in the transition regime (orange in Figure 7).

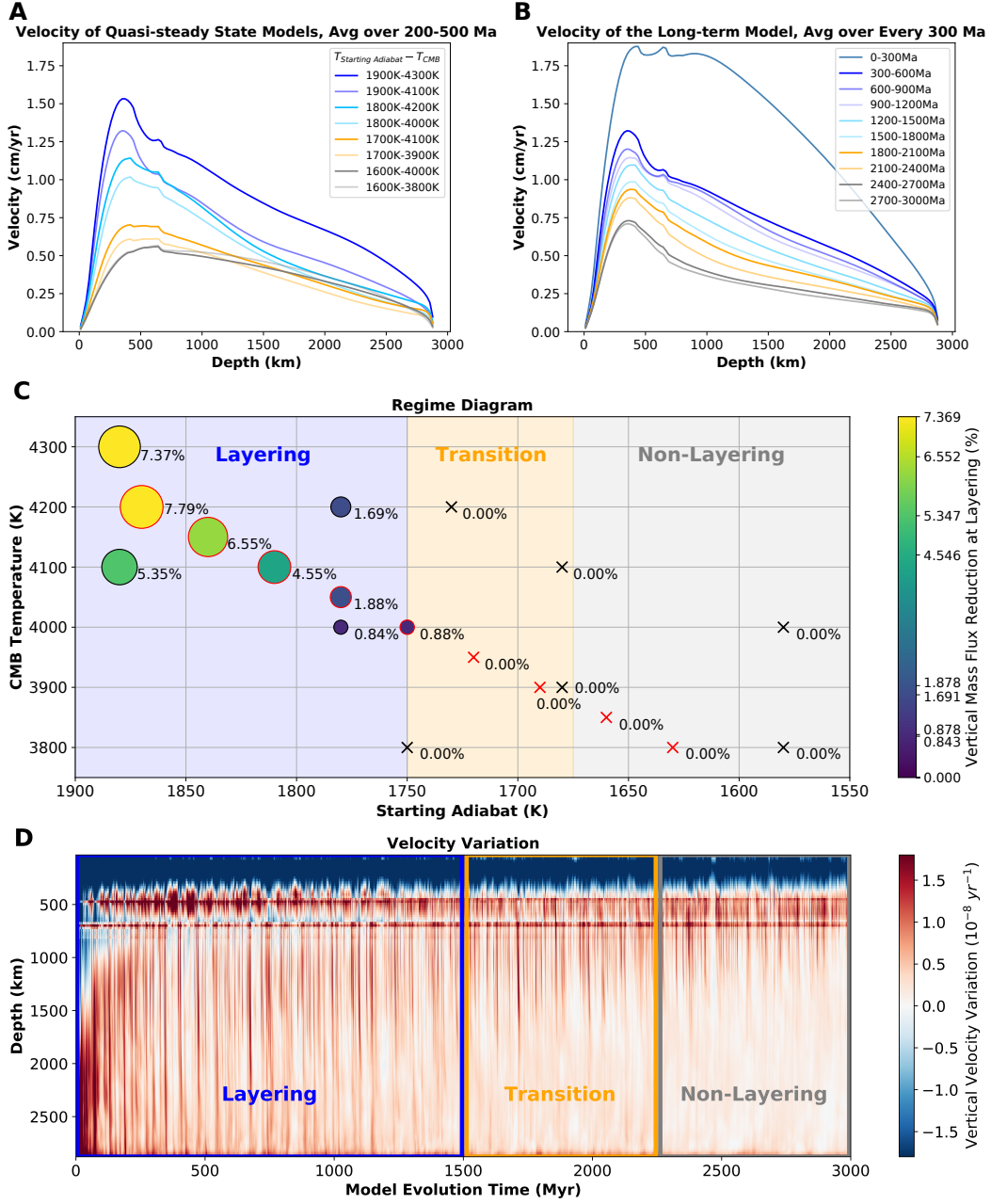


**Figure 6.** A: Averaged vertical velocity vs. depth. Blue, orange and grey lines are model periods that fall into the layering regime, transition regime, and non-layering regime, respectively. In A, each line represents a different quasi-steady state model with the velocity being averaged over the time period of 200-500 Myr. In B, each line represents an average over a period of 300 Myr in the long-term model 1900-cools. C: Regime diagram. Circle size and color indicate each model's mass flux reduction in dependence of its mantle potential temperature and CMB temperature. Circles with a black outline are calculated from the quasi-steady state models, each averaged over the model evolution time of 200-500 Myr. As these models cool around 10 K per 100 Myr, they are plotted at a temperature that is 20 K below their starting adiabat. Circles outlined in red represent averages over a 300-Myr-period of the long-term model. D: Spatial derivative of the vertical velocity, i.e. velocity variation with depth. Blue colors indicate rising material that is slowing down due to an effect that impedes upwards flow.

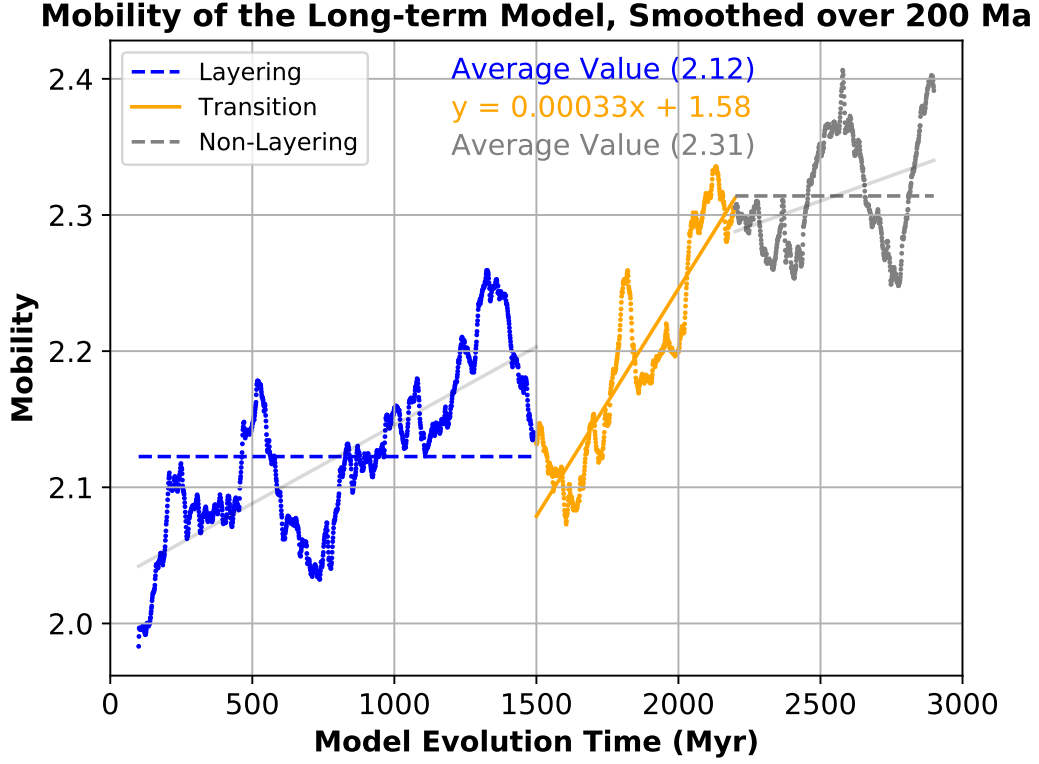


**Figure 7.** Changes in mobility over time in model 1900-cools. Mobility is calculated as the ratio of surface RMS velocity to whole model RMS velocity. Model evolution time falling into the layering regime is plotted in blue; the transition regime is plotted in orange; the non-layering regime is plotted in grey. The blue and grey dashed lines show the average mobility in those two time periods. Solid lines highlight a linear fit to the mobility in each of the three time periods, revealing a significantly flatter slope in the layering and non-layering regime compared to the increasing trend of the transition regime (orange solid line).

Surface mobility quantifies the extent to which the lithosphere is able to move compared to the underlying mantle, and it is an indicator for tectonic regimes (Tackley, 2000b). The smaller surface mobility suggests more sluggish plate tectonics compared to the mantle flow when layering occurs. We suggest that the cause for this relation is the impact of plumes on plate tectonics: In the layering regime, some plumes stagnate partially or completely between 500 km and 600 km depth. As fewer plumes reach the surface, plume–lithosphere interaction is less frequent and weaker in the layering regime. Since plumes impose stresses to the base of the lithosphere and have even been linked to continental break-up, the absence or reduction of these interactions results in less plume-induced surface movement. Note, however, that the average plate velocity still decreases over time due to the lower convective vigor for lower mantle temperatures—so this change signifies a more sluggish plate motion compared to the mantle flow, not in the absolute speed.

The geological record suggests that there have been changes in the style of plate tectonics throughout Earth’s secular cooling (Korenaga, 2013; Palin et al., 2020). Subduction-driven mobile lid style convection may have been widely established by the Mid-Archean, followed by a period of time (1.7 Ga–0.75 Ga, the “boring billion” (Cawood & Hawkesworth, 2014)) with a low amount of subduction-related petrological records. The Earth’s mantle then transitioned to the modern-style subduction regime. Since the mantle temperature significantly affects lithosphere dynamics (Sizova et al., 2014), and our models reveal that the layering of plumes can both increase the transition zone temperature and change the convection style, the layering induced by the wadsleyite to garnet (majorite) + ferropericlase transition may have been one of the factors that contributed to this change in surface tectonics.

#### 4.4 Melt Generation in the Layered Plume Heads

We also track where in the model the temperature and pressure cross the dry pyroxene solidus presented in Stixrude et al. (2009). The heads of many plumes that rise in the layering regime can cross the solidus already in the transition zone. Amongst these plumes that generate melts when their heads reach the transition zone, the majority rise straight up towards the base of the lithosphere rather than being deflected. However, some of these partially molten plume heads are completely stagnant at 500 to 600 km depth. These plume heads spread out horizontally in the transition zone. Later on, this hot material spawns secondary plumes that rise at a different horizontal location (see Figure A2 in the Appendix). During this process, the plumes may leave the generated melt behind in the transition zone, for example if the melt was able to migrate (upwards or downwards, depending on its density) away from its source location while the plume head is spreading horizontally. Without further constraints on the proportion and density of these partial melts, we can not predict their final destination. However, this process could differentiate the plume chemically, and contribute to mantle heterogeneity.

#### 4.5 Effect of Olivine to Wadsleyite Transition and Post-Spinel Transition

The olivine to wadsleyite phase transition, which occurs at around 410 km depth in today’s Earth and around 450 km depth along a 1900 K adiabat has a positive Clapeyron slope. Heat diffusion at this exothermic transition causes a decrease of entropy. In our models, we observe a density change that can accelerate both slabs and plumes. However, the increase of velocity is not obvious and therefore the dynamic effect is hard to quantify.

Another important phase transition in the mantle is the post-spinel phase transition, which occurs at around 660 km depth. Many observations suggest that some slabs can stagnate at the post-spinel transition (Goes et al., 2017). In our models, however, most slabs can penetrate through the transition zone. The stagnation effect of a phase

transition on subducted slabs in general depends on its buoyancy parameter. Christensen and Yuen (1985) define the phase buoyancy parameter  $P = \gamma\Delta\rho/(\rho\alpha\Delta T)$ , and suggest that only phase transitions with  $P$  below the critical phase buoyancy parameter,  $P_{critical}$ , may induce fully layered convection.  $P_{critical}$  depends on the Rayleigh number ( $Ra$ ) of the model, and can be estimated by the empirical equation  $P_{critical} = -4.4Ra^{-0.2}$  (Eq. 25 in Christensen and Yuen (1985)). Therefore, assuming  $Ra$  approximately equal to  $1.8 \times 10^7$  (estimated with  $\alpha = 3 \times 10^{-5}$ ,  $\rho = 5000 \text{ kg/m}^3$ ,  $\eta = 10^{22} \text{ Pa s}$ ,  $C_p = 1250 \text{ J/kg/K}$ ) in our model that represents the present-day Earth, the post-spinel phase transition, which has  $\Delta\rho$  around  $200 \text{ kg/m}^3$ , may cause completely layered convection only if it has a Clapeyron slope more negative than  $-16.9 \text{ MPa/K}$ . However, the Clapeyron slope of the post-spinel phase transition in our pyrolite assemblage is around  $-1.4 \text{ MPa/K}$ , which is far below the threshold. Therefore, the effect of the transition is not strong enough to lead to layering, but it still impacts some subducted slabs.

The trench retreat at the surface also plays an important role for the effect of phase transitions on subducted slabs. We observe that slabs flatten and stagnate in the transition zone at the beginning of the models with the present-day mantle adiabat. Such stagnation is not a common feature and rarely occurs later during the model evolution. This is because for the very first subduction zones that have extremely thick and strong slabs, the trench retreat rate is fast, leading to a shallow dipping angle and enhancing the resistance of the phase transformation (Christensen, 1996). At later times, when the convection cycle and plate tectonics are already established, the trench retreat rate becomes smaller. Slabs tend to subduct at higher angles and penetrate the post-spinel phase transition. In addition, slabs show buckling as soon as they reach 660 km depth due to the viscosity increase in the lower mantle.

We also note that the  $ri \rightarrow bg + fp$  transition with this negative Clapeyron slope is only present for average and subducted slab geotherms (for the present-day), but not for higher temperatures such as in mantle plumes or earlier in Earth's history (see red stripe around 660 km depth in Figure 1, right). It therefore does not have a layering effect on plumes.

#### 4.6 Limitations and Future Directions

This study has a few considerable limitations that future studies can further address.

1. Although we have discussed the potential occurrence of melt pockets in the layered plumes, we do not include the effect of melting or melt migration in our models. On the one hand, geodynamic modeling has suggested that melt production at mid-ocean ridges is controlled by surface plate motions (M. Li et al., 2016). In our models, the secular cooling of the mantle and the change from a layering to a non-layering regime may affect the melt production at the surface. On the other hand, melting of the mantle at mid-ocean ridges can also affect the thickness and rheology of plates (Hirth & Kohlstedt, 1996). A higher melting degree from hotter mantle potential temperatures can therefore form slabs with greater negative buoyancy forces (Weller et al., 2019). Such effects potentially affect the vigor of convection and the speed of plate motion.
2. Our 2-D cylindrical annulus model setup has geometrical limitations, especially for the plume morphology. The head-to-conduit ratio of plumes in 3-D is larger than for plumes in 2-D. Such a difference is not likely to affect the existence of layering, but it can potentially affect the amount of layered material, which would be underestimated in our models.
3. Our models have a homogeneous pyrolitic composition due to the limitations of the entropy formulation. An advance in the entropy method that incorporates mul-

multiple components is required to reveal the evolution of mantle heterogeneity, such as oceanic crust segregation.

4. We prescribed the cooling rate of the core-mantle boundary. A coupled core-mantle model with self-consistent cooling of the CMB would be a more realistic representation of the temperature evolution of the Earth through time.
5. Our models do not have continents. Although the continental insulation may not affect the global heat flow, the thermal blanket effect of the continents can produce localized weakening (Lenardic et al., 2005). Previous studies have suggested that stable continents can affect the convection regime and facilitate subduction at higher surface yield strength (Rolf & Tackley, 2011).

However, these limitations do not affect the main results of our study, a change from layering to a non-layering regime induced by the wadsleyite to garnet (majorite) + ferropericlasite phase transformation during Earth’s secular cooling. This phase transformation and its influence on Earth’s evolution has not been widely explored before. In addition, as the first practical application of the entropy method (Dannberg et al., 2022) on global mantle convection modeling, we demonstrate the usefulness and feasibility of integrating an Earth-like mantle rheology with this new method for modeling phase transitions in long-term geodynamic simulations.

## 5 Conclusions

We apply a recently developed entropy formulation in 2-D mantle convection models with plate tectonics to investigate the effect of phase transitions on changes in convection style throughout Earth’s history. Our models reveal the impact of the wadsleyite to garnet (majorite) + ferropericlasite endothermic transition, which occurs in a hotter mantle early in Earth’s evolution and impedes rising mantle plumes. When they encounter this phase transition, the plume conduits tilt heavily and the plume heads spread out laterally, forming a long-lasting global hot layer in the transition zone. The layering occurs dominantly when the mantle potential temperature is higher than 1750 K, which corresponds to times before 1.5 Ga, assuming Earth’s mantle cools by 100 K per Gyr as suggested by petrologic evidence. As Earth cools, the effect becomes weaker, but it is still noticeable for mantle potential temperatures higher than 1675 K, corresponding to 0.75 Ga.

These stalled plumes can locally raise the temperature by up to 250 K above the adiabat and globally by up to  $\sim 9.5$  K, and the layering of upwelling hot material decreases the mass exchange between lower and upper mantle by up to  $\sim 8\%$ . Since the layered plume heads are hot enough for partial melting to occur, and hot plume material is transported laterally within the transition zone before spawning secondary plumes at a new location, this process likely leads to chemical differentiation within the plume. In addition, the surface mobility of our model increases significantly during the transition from a layering to a non-layering convection regime, suggesting that the change in mantle flow pattern resulting from the phase transformation also affects surface plate tectonics, causing the surface to move faster compared to the mantle. Our results demonstrate that the changes in mineral assemblage and the corresponding phase transitions during Earth’s secular cooling have an important impact not only on mantle convection style, but also on the mantle’s thermal and chemical evolution and on plate tectonics.

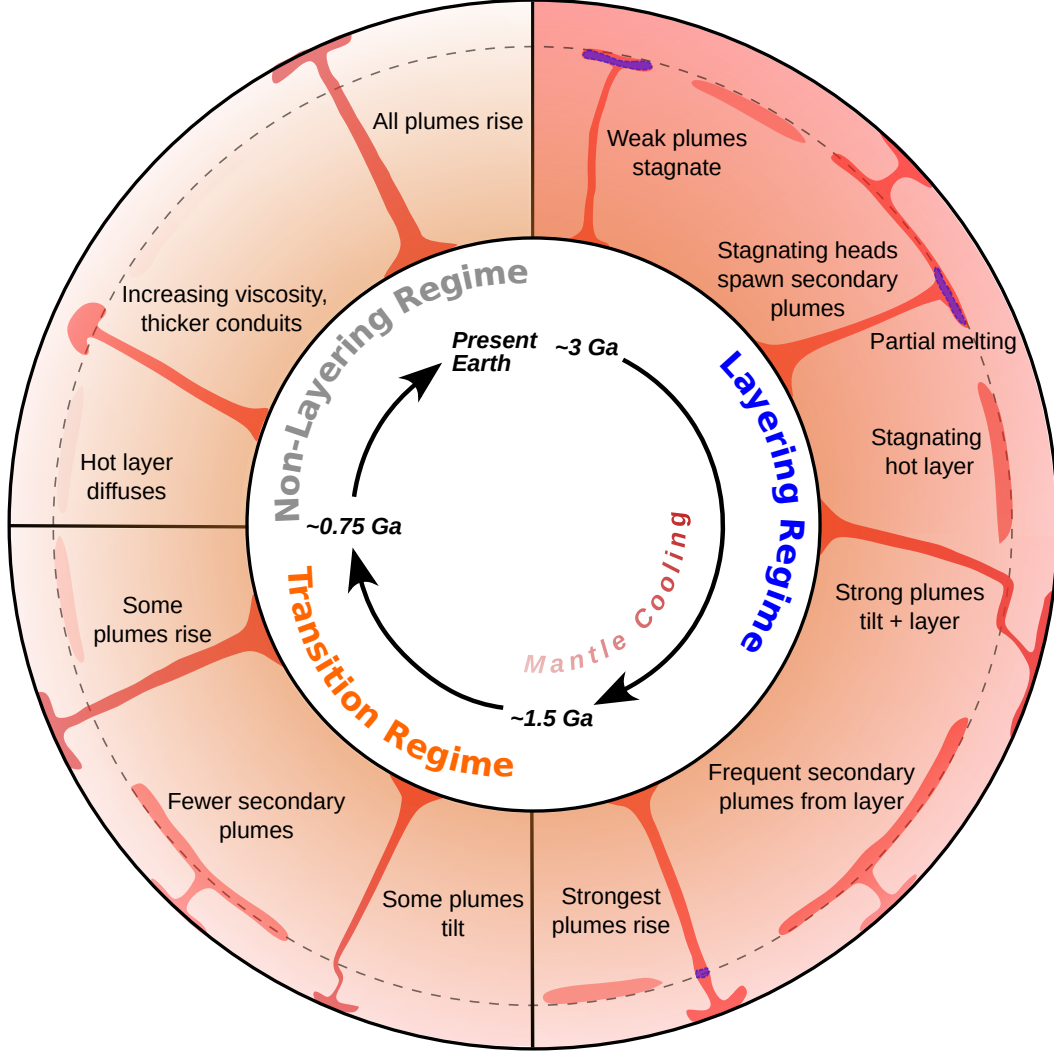


**Figure 8.** A schematic diagram summarizing the plume morphologies featured in our models and how they change throughout the Earth’s secular cooling. Time evolves in clockwise direction. The dashed line indicates a depth of 500 km, where the wadsleyite to garnet (majorite) + ferropericlase phase transformation occurs. Purple shading illustrates areas where partial melting occurs. The timeline and corresponding convection regimes assume that the mantle potential temperature was 1900 K at around 3 Ga and that the mantle cools about 100 K per Gyr.

## **Appendix A Additional figures**

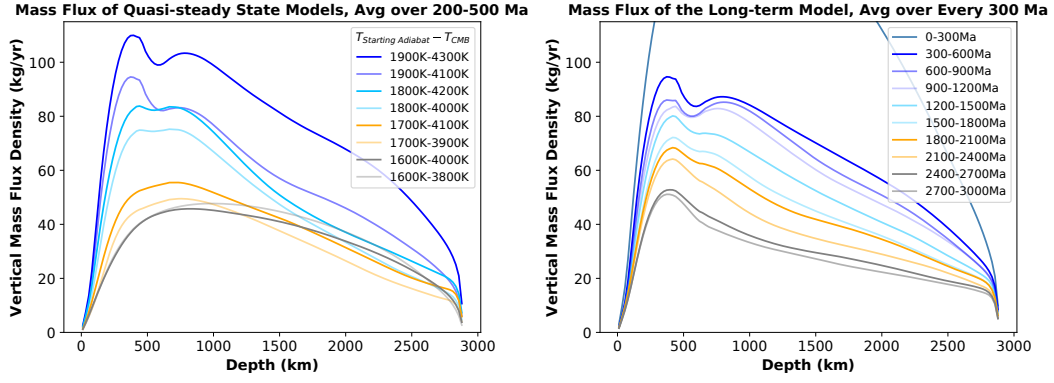


**Figure A1.** Averaged vertical mass flux density vs. depth. Note that the mass flux values from 2-D models such as this are not directly comparable to mass fluxes in a 3D mantle. Blue, orange and grey lines are model periods that fall into the layering regime, transition regime, and non-layering regime, respectively. Left: Each line represents a different quasi-steady state model with the vertical mass flux being averaged over the time period of 200-500 Myr. Right: Each line represents an average over a period of 300 Myr in the long-term model 1900-cools.

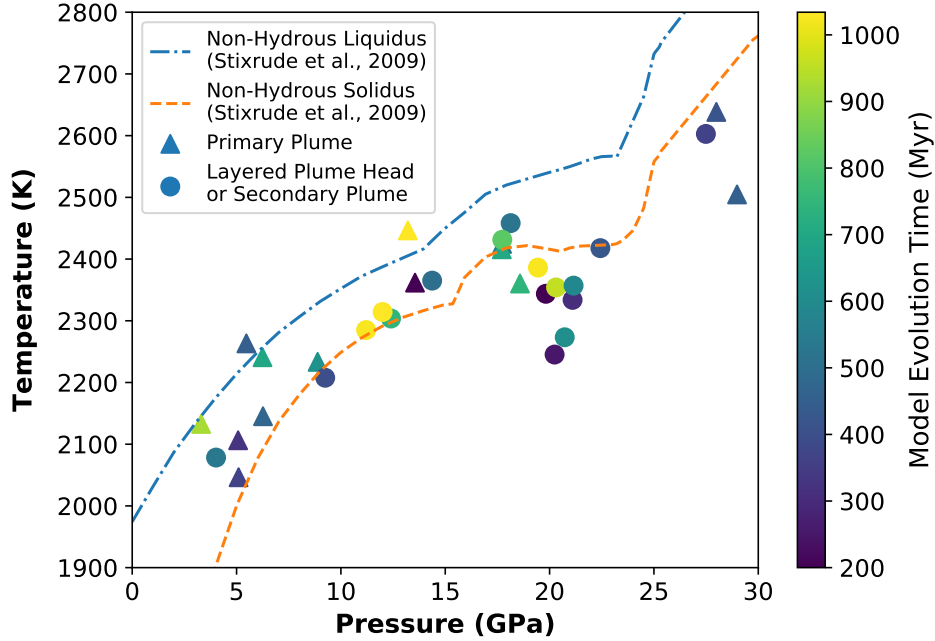


**Figure A2.** Plume temperature vs. depth, illustrating where partial melting would occur. Colored symbols represent temperatures within plumes generated in the 1900-cools model. Triangles are points located in plumes which rise straight up to the surface. Circles are points located within layered plume heads or secondary plumes. The color of each symbol represents the model evolution time at which these points are selected. The dashed lines indicate the solidus and liquidus of dry pyrolite from Stixrude et al. (2009).

## Acknowledgments

The authors acknowledge support by NSF award EAR 1925677—Development and Application of a Framework for Integrated Geodynamic Earth Models. JD and RG were also partially supported by NSF awards EAR 2054605 and 2149126. ASPECT is hosted by the Computational Infrastructure for Geodynamics (CIG) which is supported by the National Science Foundation awards EAR 1550901 and 2149126. The authors also acknowledge the University of Florida Research Computing (<https://www.rc.ufl.edu/>) for providing computational resources and support that have contributed to the research results reported in this publication.

## Open Research

The code modifications, parameter, data, and log files used for the models in the study are available on Zenodo at DOI 10.5281/zenodo.10732675 under the MIT licence (Li et al., 2024).

ASPECT version 2.6.0-pre (commit hash 6713edf45), (Heister et al., 2017; Kronbichler et al., 2012; Bangerth et al., 2023b, 2023a; Clevenger & Heister, 2021; Gassmöller et al., 2020)) used in these computations is freely available under the GPL v2.0 or later license through its software landing page <https://geodynamics.org/resources/aspect> or <https://aspect.geodynamics.org> and is being actively developed on GitHub and can be accessed via <https://github.com/geodynamics/aspect>. The code HeFESTo is available on GitHub at <https://github.com/stixrude/HeFESToRepository>.

## References

- Allègre, C. J. (1997). Limitation on the mass exchange between the upper and lower mantle: the evolving convection regime of the earth. *Earth and Planetary Science Letters*, 150(1-2), 1–6.
- Artemieva, I. M. (2006). Global  $1 \times 1$  thermal model tc1 for the continental lithosphere: implications for lithosphere secular evolution. *Tectonophysics*, 416(1-4), 245–277.
- Ballmer, M. D., Houser, C., Hernlund, J. W., Wentzcovitch, R. M., & Hirose, K. (2017). Persistence of strong silica-enriched domains in the earth’s lower mantle. *Nature Geoscience*, 10(3), 236–240.
- Bangerth, W., Dannberg, J., Fraters, M., Gassmoeller, R., Glerum, A., Heister, T., ... Naliboff, J. (2023a, July). *ASPECT: Advanced Solver for Problems in Earth’s ConvecTion, User Manual*. Retrieved from <https://doi.org/10.6084/m9.figshare.4865333> (doi:10.6084/m9.figshare.4865333) doi: 10.6084/m9.figshare.4865333
- Bangerth, W., Dannberg, J., Fraters, M., Gassmoeller, R., Glerum, A., Heister, T., ... Naliboff, J. (2023b, July). *Aspect v2.5.0*. Zenodo. Retrieved from <https://doi.org/10.5281/zenodo.8200213> doi: 10.5281/zenodo.8200213
- Becker, T. W., Kellogg, J. B., & O’Connell, R. J. (1999). Thermal constraints on the survival of primitive blobs in the lower mantle. *Earth and Planetary Science Letters*, 171(3), 351–365.
- Bercovici, D., & Karato, S.-i. (2003). Whole-mantle convection and the transition-zone water filter. *Nature*, 425(6953), 39–44.
- Bossmann, A. B., & van Keken, P. E. (2013). Dynamics of plumes in a compressible mantle with phase changes: Implications for phase boundary topography. *Physics of the Earth and Planetary Interiors*, 224, 21–31.
- Brandenburg, J., Hauri, E. H., van Keken, P. E., & Ballentine, C. J. (2008). A multiple-system study of the geochemical evolution of the mantle with force-balanced plates and thermochemical effects. *Earth and Planetary Science Letters*, 276(1-2), 1–13.

- Brown, M., & Johnson, T. (2018). Secular change in metamorphism and the onset of global plate tectonics. *American Mineralogist*, 103(2), 181–196.
- Brunet, D., & Yuen, D. A. (2000). Mantle plumes pinched in the transition zone. *Earth and Planetary Science Letters*, 178(1-2), 13–27.
- Burgos, G., Montagner, J.-P., Beucler, E., Capdeville, Y., Mocquet, A., & Drilleau, M. (2014). Oceanic lithosphere-asthenosphere boundary from surface wave dispersion data. *Journal of Geophysical Research: Solid Earth*, 119(2), 1079–1093.
- Cawood, P. A., & Hawkesworth, C. J. (2014). Earth’s middle age. *Geology*, 42(6), 503–506.
- Christensen, U. R. (1996). The influence of trench migration on slab penetration into the lower mantle. *Earth and Planetary Science Letters*, 140(1-4), 27–39.
- Christensen, U. R., & Yuen, D. A. (1984). The interaction of a subducting lithospheric slab with a chemical or phase boundary. *Journal of Geophysical Research: Solid Earth*, 89(B6), 4389–4402.
- Christensen, U. R., & Yuen, D. A. (1985). Layered convection induced by phase transitions. *Journal of Geophysical Research: Solid Earth*, 90(B12), 10291–10300.
- Clevenger, T. C., & Heister, T. (2021, March). Comparison between algebraic and matrix-free geometric multigrid for a Stokes problem on an adaptive mesh with variable viscosity. *Numerical Linear Algebra with Applications*. Retrieved from <https://arxiv.org/abs/1907.06696> doi: 10.1002/nla.2375
- Condie, K. C., Aster, R. C., & Van Hunen, J. (2016). A great thermal divergence in the mantle beginning 2.5 ga: Geochemical constraints from greenstone basalts and komatiites. *Geoscience Frontiers*, 7(4), 543–553.
- Dannberg, J., Gassmöller, R., Li, R., Lithgow-Bertelloni, C., & Stixrude, L. (2022). An entropy method for geodynamic modelling of phase transitions: capturing sharp and broad transitions in a multiphase assemblage. *Geophysical Journal International*, 231(3), 1833–1849.
- Dasgupta, R., Hirschmann, M. M., & Smith, N. D. (2007). Partial melting experiments of peridotite+ co<sub>2</sub> at 3 gpa and genesis of alkalic ocean island basalts. *Journal of Petrology*, 48(11), 2093–2124.
- Faccenda, M., & Dal Zilio, L. (2017). The role of solid–solid phase transitions in mantle convection. *Lithos*, 268, 198–224.
- French, S. W., & Romanowicz, B. (2015). Broad plumes rooted at the base of the earth’s mantle beneath major hotspots. *Nature*, 525(7567), 95–99.
- Gassmöller, R., Dannberg, J., Bangerth, W., Heister, T., & Myhill, R. (2020). On formulations of compressible mantle convection. *Geophysical Journal International*, 221(2), 1264–1280. Retrieved from <https://doi.org/10.1093/gji/ggaa078> doi: 10.1093/gji/ggaa078
- Goes, S., Agrusta, R., van Hunen, J., & Garel, F. (2017). Subduction-transition zone interaction: A review. *Geosphere*, 13(3), 644–664.
- Graham, D. W. (2002). Noble gas isotope geochemistry of mid-ocean ridge and ocean island basalts: Characterization of mantle source reservoirs.
- Gülcher, A. J. P., Ballmer, M. D., & Tackley, P. J. (2021). Coupled dynamics and evolution of primordial and recycled heterogeneity in earth’s lower mantle. *Solid Earth*, 12(9), 2087–2107.
- Heister, T., Dannberg, J., Gassmöller, R., & Bangerth, W. (2017). High accuracy mantle convection simulation through modern numerical methods. II: Realistic models and problems. *Geophysical Journal International*, 210(2), 833–851. Retrieved from <https://doi.org/10.1093/gji/ggx195> doi: 10.1093/gji/ggx195
- Herzberg, C., Condie, K., & Korenaga, J. (2010). Thermal history of the earth and its petrological expression. *Earth and Planetary Science Letters*, 292(1-2), 79–88.

- Hirth, G., & Kohlstedt, D. L. (1996). Water in the oceanic upper mantle: implications for rheology, melt extraction and the evolution of the lithosphere. *Earth and Planetary Science Letters*, 144(1-2), 93–108.
- Hofmann, A. W. (1988). Chemical differentiation of the earth: the relationship between mantle, continental crust, and oceanic crust. *Earth and Planetary Science Letters*, 90(3), 297–314.
- Hofmann, A. W. (1997). Mantle geochemistry: the message from oceanic volcanism. *Nature*, 385(6613), 219–229.
- Hofmann, A. W., & White, W. M. (1982). Mantle plumes from ancient oceanic crust. *Earth and Planetary Science Letters*, 57(2), 421–436.
- Ichikawa, H., Kameyama, M., Senshu, H., Kawai, K., & Maruyama, S. (2014). Influence of majorite on hot plumes. *Geophysical Research Letters*, 41(21), 7501–7507.
- Jackson, M. G., Carlson, R. W., Kurz, M. D., Kempton, P. D., Francis, D., & Blusztajn, J. (2010). Evidence for the survival of the oldest terrestrial mantle reservoir. *Nature*, 466(7308), 853–856.
- Kellogg, L. H. (1992). Mixing in the mantle. *Annual Review of Earth and Planetary Sciences*, 20(1), 365–388.
- Kellogg, L. H., Hager, B. H., & van der Hilst, R. D. (1999). Compositional stratification in the deep mantle. *Science*, 283(5409), 1881–1884.
- Korenaga, J. (2013). Initiation and evolution of plate tectonics on earth: theories and observations. *Annual review of earth and planetary sciences*, 41, 117–151.
- Korenaga, J. (2017). Pitfalls in modeling mantle convection with internal heat production. *Journal of Geophysical Research: Solid Earth*, 122(5), 4064–4085.
- Kronbichler, M., Heister, T., & Bangerth, W. (2012). High accuracy mantle convection simulation through modern numerical methods. *Geophysical Journal International*, 191, 12–29. Retrieved from <http://dx.doi.org/10.1111/j.1365-246X.2012.05609.x> doi: 10.1111/j.1365-246X.2012.05609.x
- Lenardic, A., Moresi, L.-N., Jellinek, A., & Manga, M. (2005). Continental insulation, mantle cooling, and the surface area of oceans and continents. *Earth and Planetary Science Letters*, 234(3-4), 317–333.
- Li, M., Black, B., Zhong, S., Manga, M., Rudolph, M. L., & Olson, P. (2016). Quantifying melt production and degassing rate at mid-ocean ridges from global mantle convection models with plate motion history. *Geochemistry, Geophysics, Geosystems*, 17(7), 2884–2904.
- Li, R., Dannberg, J., Gassmöller, R., Lithgow-Bertelloni, C., & Stixrude, L. (2024, March). *Exploring Mantle Convection Styles through Earth's History: The Role of Phase Transitions: Data*. Zenodo. Retrieved from <https://doi.org/10.5281/zenodo.10732675> doi: 10.5281/zenodo.10732675
- Liu, H., Wang, W., Jia, X., Leng, W., Wu, Z., & Sun, D. (2018). The combined effects of post-spinel and post-garnet phase transitions on mantle plume dynamics. *Earth and Planetary Science Letters*, 496, 80–88.
- Lourenço, D. L., Rozel, A. B., Ballmer, M. D., & Tackley, P. J. (2020). Plutonic-squishy lid: a new global tectonic regime generated by intrusive magmatism on earth-like planets. *Geochemistry, Geophysics, Geosystems*, 21(4), e2019GC008756.
- Machetel, P., & Weber, P. (1991). Intermittent layered convection in a model mantle with an endothermic phase change at 670 km. *Nature*, 350(6313), 55–57.
- Manga, M. (1996). Mixing of heterogeneities in the mantle: Effect of viscosity differences. *Geophysical Research Letters*, 23(4), 403–406.
- Marquart, G., Schmeling, H., Ito, G., & Schott, B. (2000). Conditions for plumes to penetrate the mantle phase boundaries. *Journal of Geophysical Research: Solid Earth*, 105(B3), 5679–5693.
- Naliboff, J. B., & Kellogg, L. H. (2007). Can large increases in viscosity and thermal conductivity preserve large-scale heterogeneity in the mantle? *Physics of*

- the *Earth and Planetary Interiors*, 161(1-2), 86–102.
- O'Neill, C., Lenardic, A., & Condie, K. (2015). Earth's punctuated tectonic evolution: cause and effect. *Geological Society, London, Special Publications*, 389(1), 17–40.
- Palin, R. M., Santosh, M., Cao, W., Li, S.-S., Hernández-Urbe, D., & Parsons, A. (2020). Secular change and the onset of plate tectonics on earth. *Earth-Science Reviews*, 207, 103172.
- Peltier, W., & Solheim, L. (1992). Mantle phase transitions and layered chaotic convection. *Geophysical Research Letters*, 19(3), 321–324.
- Richter, F., McKenzie, D., et al. (1977). Simple plate models of mantle convection. *Journal of Geophysics*, 44(1), 441–471.
- Roberts, N. M., & Spencer, C. J. (2015). The zircon archive of continent formation through time..
- Rolf, T., & Tackley, P. (2011). Focussing of stress by continents in 3d spherical mantle convection with self-consistent plate tectonics. *Geophysical Research Letters*, 38(18).
- Rychert, C. A., Harmon, N., Constable, S., & Wang, S. (2020). The nature of the lithosphere-asthenosphere boundary. *Journal of Geophysical Research: Solid Earth*, 125(10), e2018JB016463.
- Sizova, E., Gerya, T., & Brown, M. (2014). Contrasting styles of phanerozoic and precambrian continental collision. *Gondwana Research*, 25(2), 522–545.
- Solomatov, V. (1995). Scaling of temperature-and stress-dependent viscosity convection. *Physics of Fluids*, 7(2), 266–274.
- Steinberger, B., & Calderwood, A. R. (2006). Models of large-scale viscous flow in the earth's mantle with constraints from mineral physics and surface observations. *Geophysical Journal International*, 167(3), 1461–1481.
- Stixrude, L., de Koker, N., Sun, N., Mookherjee, M., & Karki, B. B. (2009). Thermodynamics of silicate liquids in the deep earth. *Earth and Planetary Science Letters*, 278(3-4), 226–232.
- Stixrude, L., & Lithgow-Bertelloni, C. (2005). Thermodynamics of mantle minerals—i. physical properties. *Geophysical Journal International*, 162(2), 610–632.
- Stixrude, L., & Lithgow-Bertelloni, C. (2011). Thermodynamics of mantle minerals—ii. phase equilibria. *Geophysical Journal International*, 184(3), 1180–1213.
- Stixrude, L., & Lithgow-Bertelloni, C. (2022). Thermal expansivity, heat capacity and bulk modulus of the mantle. *Geophysical Journal International*, 228(2), 1119–1149.
- Sun, S.-S., & McDonough, W. F. (1989). Chemical and isotopic systematics of oceanic basalts: implications for mantle composition and processes. *Geological Society, London, Special Publications*, 42(1), 313–345.
- Tackley, P. J. (2000a). Mantle convection and plate tectonics: Toward an integrated physical and chemical theory. *Science*, 288(5473), 2002–2007.
- Tackley, P. J. (2000b). Self-consistent generation of tectonic plates in time-dependent, three-dimensional mantle convection simulations. *Geochemistry, Geophysics, Geosystems*, 1(8).
- Tackley, P. J., Stevenson, D. J., Glatzmaier, G. A., & Schubert, G. (1993). Effects of an endothermic phase transition at 670 km depth in a spherical model of convection in the earth's mantle. *Nature*, 361(6414), 699–704.
- Tosi, N., & Yuen, D. A. (2011). Bent-shaped plumes and horizontal channel flow beneath the 660 km discontinuity. *Earth and Planetary Science Letters*, 312(3-4), 348–359.
- van Keken, P. E., & Ballentine, C. J. (1999). Dynamical models of mantle volatile evolution and the role of phase transitions and temperature-dependent rheology. *Journal of Geophysical Research: Solid Earth*, 104(B4), 7137–7151.
- van Keken, P. E., Hauri, E. H., & Ballentine, C. J. (2002). Mantle mixing: the gen-

- eration, preservation, and destruction of chemical heterogeneity. *Annual Review of Earth and Planetary Sciences*, 30(1), 493–525.
- van Keken, P. E., & Zhong, S. (1999). Mixing in a 3d spherical model of present-day mantle convection. *Earth and Planetary Science Letters*, 171(4), 533–547.
- Weaver, B. L. (1991). The origin of ocean island basalt end-member compositions: trace element and isotopic constraints. *Earth and planetary science letters*, 104(2-4), 381–397.
- Wei, S. S., Shearer, P. M., Lithgow-Bertelloni, C., Stixrude, L., & Tian, D. (2020). Oceanic plateau of the hawaiian mantle plume head subducted to the uppermost lower mantle. *Science*, 370(6519), 983–987.
- Weis, D., Harpp, K. S., Harrison, L. N., Boyet, M., Chauvel, C., Farnetani, C. G., ... others (2023). Earth’s mantle composition revealed by mantle plumes. *Nature Reviews Earth & Environment*, 1–22.
- Weller, O., Copley, A., Miller, W., Palin, R., & Dyck, B. (2019). The relationship between mantle potential temperature and oceanic lithosphere buoyancy. *Earth and planetary science letters*, 518, 86–99.
- White, W. M. (2010). Oceanic island basalts and mantle plumes: the geochemical perspective. *Annual Review of Earth and Planetary Sciences*, 38, 133–160.
- White, W. M. (2015). Probing the earth’s deep interior through geochemistry. *Geochemical Perspectives*, 4(2).
- Xie, S., & Tackley, P. J. (2004). Evolution of u-pb and sm-nd systems in numerical models of mantle convection and plate tectonics. *Journal of Geophysical Research: Solid Earth*, 109(B11).
- Xu, W., Lithgow-Bertelloni, C., Stixrude, L., & Ritsema, J. (2008). The effect of bulk composition and temperature on mantle seismic structure. *Earth and Planetary Science Letters*, 275(1-2), 70–79.
- Zahirovic, S., Müller, R. D., Seton, M., & Flament, N. (2015). Tectonic speed limits from plate kinematic reconstructions. *Earth and Planetary Science Letters*, 418, 40–52.
- Zindler, A., & Hart, S. (1986). Chemical geodynamics. *Annual review of earth and planetary sciences*, 14(1), 493–571.